NASA/TM—1998-206629

Stability of Capillary Surfaces in Rectangular Containers: The Right Square Cylinder

M. M. Weislogel and K.C. Hsieh
Lewis Research Center, Cleveland, Ohio

National Aeronautics and
Space Administration

Lewis Research Center

January 1998

This report contains preliminary findings, subject to revision as analysis proceeds.

Available from

NASA Center for Aerospace Information
800 Elkridge Landing Road
Linthicum Heights, MD 21090-2934
Price Code: A03

National Technical Information Service
5287 Port Royal Road
Springfield, VA 22100
Price Code: A03

STABILITY OF CAPILLARY SURFACES IN RECTANGULAR CONTAINERS: THE RIGHT SQUARE CYLINDER

Mark M. Weislogel and K.C. Hsieh
NASA Lewis Research Center M.S. 500/102
Cleveland, OH 44135

Abstract

The linearized governing equations for an ideal fluid are presented for numerical analysis for the stability of free capillary surfaces in rectangular containers against unfavorable disturbances (accelerations, *i.e.* Rayleigh-Taylor instability). The equations are solved for the case of the right square cylinder. The results are expressed graphically in terms of a critical Bond number as a function of system contact angle. A critical wetting phenomena in the corners is shown to significantly alter the region of stability for such containers in contrast to simpler geometries such as the right circular cylinder or the infinite rectangular slot. Such computational results provide additional constraints for the design of fluids systems for space-based applications.

INTRODUCTION

Particularly since the inception of space flight a number of studies have been conducted to identify the stability limits of capillary surfaces to unfavorable disturbances (accelerations). The motivation for such investigations is generally to obtain design characteristics and performance limitations for in-space fluids management systems. For example, it is essential to understand the potentially destabilizing effects of a thruster firing on the liquid fuel in a partially-filled tank. In this paper a brief review of interfacial stability of the Rayleigh-Taylor-type will be provided which focuses on the restricted set of container geometries for which solutions are offered in the literature. In light of the growing need for design specific solutions for an ever increasing number of fluids systems applications, *i.e.* fluids experiments in space (Singh 1996), a new problem is outlined and solved for the stability of capillary surfaces in containers of rectangular cross-section. The results of this investigation, presented in terms of a critical Bond number as a function of contact angle and easily extendable to include container aspect ratio, may be readily added to the repertoire of the space systems designer.

Review

Surface tension forces dominate fluid interface behavior for low Bond number systems, $B \ll 1$, where

$$B \equiv \frac{\rho g R^2}{\sigma},$$

R_i/R_o	C_1	C_2
0	0.81	2.59
0.1	1.30	1.99
0.25	1.83	0.83
0.5	0.22	1.39
0.75	0.28	1.01
1.0	0.74	0.41

Table 1: Correlation constants for eq. 3.

where ρ is the density difference across the interface, σ is the surface or interfacial tension, R is a characteristic dimension of the container, and g is the acceleration field strength. As B approaches $O(1)$, however, a critical balance is reached and, depending on the orientation of the acceleration field, further increases in g can cause destabilization of the interface and reorientation of the fluid to a perhaps undesirable location within the container. The precise value of B at which such a "reorientation" might occur ($\equiv B_{cr}$) is an important design parameter for any capillarity-controlled fluid system and is particularly significant for fluids management processes in space.

Critical Bond number analyses for confined geometries were performed indirectly as early as Duprez (1854) and Maxwell (1890) for the stability of pinned interfaces in circular and rectangular containers. These investigations are restricted to predominately flat surfaces originating out of an assumption of either a 90° contact angle condition or a pinned contact line. Treating the contact angle as a parameter and thus allowing significant curvature of the interface, as is most common in capillary systems, solutions were obtained by Concus (1968) for the right circular cylinder, Concus (1963) for the infinite slot, and Seebold *et al.* (1967) for the circular annulus. The experimental works of Masica *et al.* (1964) and Masica and Petrash (1965) concerning the cylinder and Labus (1969) concerning the annulus are also noteworthy. Solutions for spherical containers are presented by Reynolds and Satterlee (1966) and a number of solutions are reported for semi-bounded surfaces such as wall bound drops and bubbles by Reynolds and Satterlee (1966), pedant drops by Wente (1980), and liquid bridges by Coriell *et al.* (1977). Unbounded liquid layers are treated by Yiantsios and Higgins (1989) with pertinent references contained therein.

Numerical correlations for B_{cr} as a function of the contact angle may be derived from the work of Concus (1963 and 1968) and Seebold et al. (1967), respectively. For the infinite rectangular slot one finds

$$B_{cr} = 0.71 + 1.74 \sin\theta, \tag{1}$$

where B_{cr} is defined using the slot half-width, and for the cylinder

$$B_{cr} = 0.81 + 2.59 \sin\theta, \tag{2}$$

where B_{cr} is defined using the cylinder radius. Larger values $B > B_{cr}$ lead to instability and breakup of the interface. Similar results for the annulus may be obtained. However, these depend heavily of the radius ratio R_i/R_o, where R_i and R_o are the inner and outer radii, respectively. In Fig. 1, correlations for B_{cr} for free annular surfaces are plotted versus

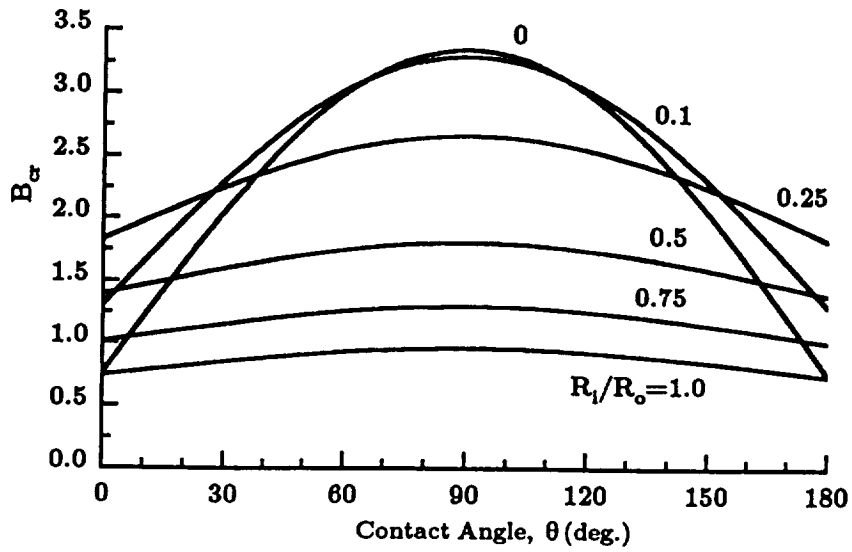

FIGURE 1. Correlations of B_{cr} with θ for annular interfaces for a variety of radius ratios, R_i/R_o (numerical data of Seebold *et al.* (1967)).

contact angle for a variety of radius ratios. The curves are determined using the form

$$B_{cr} = C_1 + C_2 \sin\theta, \tag{3}$$

and the correlation constants C_1 and C_2 are listed in Table 1. Note that B_{cr} is again defined on the outer radius, R_o, and that $R_i/R_o = 0$ recovers the correct form of eq. 3 for the circular cylinder, eq. 2. Observation of eqs. 1–3 and Fig. 1 reveals that B_{cr} is nonzero and positive for all values of the contact angle θ. In addition, the solutions are symmetric about $\theta = 90°$.

The commonality between circular cylinders, slots, and annular containers are the smooth continuous boundaries within which the fluids are confined. For the case of a container with an interior corner, the situation is altered significantly. As mathematically demonstrated by Concus and Finn (1969), when $\theta < 90° - \alpha$ (or $\theta > 180° - \alpha$), hereafter referred to as the Concus-Finn condition, a critical wetting condition is established resulting in complete wetting of the corner by the fluid: the fluid is pumped into and along the interior corners of the container by capillary forces. α is the corner half-angle. Such surfaces are unconditionally unstable to adverse accelerations. Thus, for fluid-container systems satisfying the Concus-Finn condition, $B_{cr} = 0$. Therefore, for problems such as the stability of a capillary surface in a rectangular container where $\alpha = 45°$, nonzero values for B_{cr} may only be obtained for contact angles in the range $45° < \theta < 135°$. A sketch of the different interfacial regimes is provided in Fig. 2 for a container of square cross-section. The condition of Fig. 2b ($45° < \theta < 135°$) is investigated here since the cases of Fig. 2a and 2c are unconditionally unstable for $B > 0$.

ANALYTICAL SOLUTION

Maxwell (1890) predicted the stability of an inverted capillary surface in a rectangular

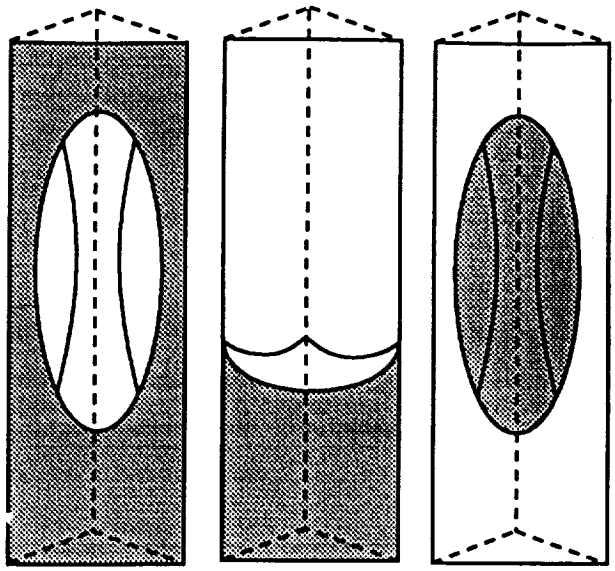

FIGURE 2. Sketch of wetting regimes in a square cross-sectioned container, liquid is shaded (note: container is bisected across diagonal): a. $\theta \leq 45°$, b. $45° < \theta < 135°$, c. $\theta \geq 135°$.

container of half-length a and half-width b. Fig. 3 depicts the geometry under discussion, where the more dense fluid is below the interface and g acts positive in the positive z-direction. Maxwell's solution is derived by minimizing the surface-plus-gravitational energy and assumes a pinned, predominately flat interface ($\theta \approx 90°$). His result may be cast in terms of B_{cr} such that

$$B_{cr} \equiv \frac{\rho g b^2}{\sigma} = \frac{\pi^2}{4}\left(1 + 4\left(\frac{b}{a}\right)^2\right), \tag{4}$$

where $0 \leq b/a \leq 1$. This solution approach may be extended to the case of perfect slip at the contact line where θ is fixed at 90°. The result is

$$B_{cr} = \frac{\pi^2}{4}\left(1 + \left(\frac{b}{a}\right)^2\right). \tag{5}$$

As is commonly observed in practice, comparison of eqs. 4 and 5 shows that stability is significantly enhanced by the pinned condition. Note also from eq. 5 that for $b/a \to 0$, $B_{cr} \to \pi^2/4$ which is equivalent to Concus' (1963) solution for the infinite slot for $\theta = 90°$ (see eq. 1), as well as to the solution for unbounded liquid layers where the disturbance wavelength $\lambda = 4b$, Yiantsios and Higgins (1989). No further analytical solutions are possible which allow appreciable variation in θ.

NUMERICAL SOLUTION

The numerical solution to the idealized equations of fluid motion are overviewed below in a like manner to Concus (1963), the dimensions of the problem being extended to analyze the surface $h = h(x, y, t)$. Conservation of mass leads to the 3-dimensional Laplace equation for the velocity potential, ϕ. The kinematic condition is applied at the free surface and the pressure jump condition across the interface due to capillary forces is then incorporated into Bernoulli's law for a transient, inviscid, incompressible, and irrotational fluid. The resulting

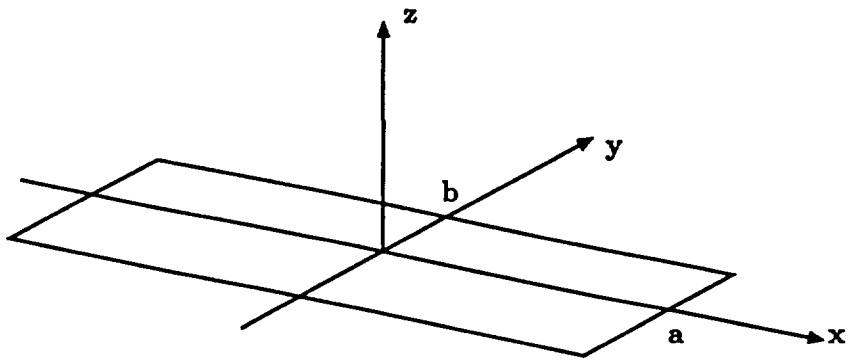

FIGURE 3. Rectangular solution domain, $a \times b$.

second order nonlinear partial differential equation is subject to the contact angle condition along the container walls. At this point the equations are linearized and normal modes are introduced for the velocity potential and for a small perturbation $\eta(x,y,t)$ to the leading order static interface shape $H(x,y;B)$. The numerical solution to the resulting governing equation requires solution to the eigenvalue problem via the evaluation of the determinant of the solution matrix for the disturbance η. A negative (positive) determinant implies growth of the disturbance and thus instability (stability). B_{cr} is determined by the zero value.

The mathematical solution detail is provided below in dimensionless form. Lengths are scaled such that $x \sim a$, $y \sim b$, $z \sim b$ and the surface height as measured from the x-y plane is $h \sim b$. Note that $\epsilon = b/a$ and that $0 \leq \epsilon \leq 1$. Time is scaled by $(b/g)^{1/2}$, pressure by σ/b, and the velocity potential by $(gb^3)^{1/2}$. Subscript notation for differentiation is employed throughout. The equations are posed for the full domain ($|x| \leq 1$, $|y| \leq 1$).

Generalized Equations

Continuity of mass leads to

$$\nabla^2 \phi = 0, \tag{6}$$

subject to $\phi_n = 0$ on the container walls, where n is the normal to the wall. The kinematic condition on the free surface is

$$\epsilon^2 \phi_x h_x + \phi_z h_z - \phi_y + h_t = 0 \tag{7}$$

on $z = h(x,y,t)$. The pressure jump condition due to curvature of the free surface is given by

$$-P = \nabla \cdot \frac{\nabla h}{\left(1 + |\nabla h|^2\right)^{1/2}} \equiv \mathcal{L}h, \tag{8}$$

where $\mathcal{L}$ is an operator on h given by

$$\mathcal{L}h \equiv \frac{\epsilon^2 h_{xx}\left(1 + h_y^2\right) + h_{yy}\left(1 + \epsilon^2 h_x^2\right) - 2\epsilon^2 h_x h_y h_{xy}}{\left(1 + \epsilon^2 h_x^2 + h_y^2\right)^{3/2}}. \tag{9}$$

The contact angle condition along the container walls is given by

$$\mathbf{n} \cdot \mathbf{k} = \cos\theta,$$

where $\mathbf{k}$ is the inward normal to the walls and $\mathbf{n}$ is the outward normal to the free surface given by

$$\mathbf{k} = (\mp 1, 0, 0) \qquad \text{along} \qquad x = \pm 1,$$
$$\mathbf{k} = (0, \mp 1, 0) \qquad \text{along} \qquad y = \pm 1,$$

and

$$\mathbf{n} = \left(1 + \epsilon^2 h_x^2 + h_y^2\right)^{-1/2} (-\epsilon h_x, -h_y, 1),$$

respectively. Thus, the contact angle conditions at the boundary of the surface are

$$\pm \frac{\epsilon h_x}{\left(1 + \epsilon^2 h_x^2 + h_y^2\right)^{1/2}} = \cos\theta \qquad \text{along} \qquad x = \pm 1 \tag{10}$$

and

$$\pm \frac{h_y}{\left(1 + \epsilon^2 h_x^2 + h_y^2\right)^{1/2}} = \cos\theta \qquad \text{along} \qquad y = \pm 1. \tag{11}$$

Incorporating eq. 8 into Bernoulli's equation for a transient, ideal fluid yields

$$B\left(\phi_t + \frac{1}{2}\left(\epsilon^2 \phi_x^2 + \phi_y^2 + \phi_z^2\right) + h\right) + \mathcal{L}h = C, \tag{12}$$

which is applicable on $z = h(x, y, t)$. C in the above equation is a constant, and in the most general sense $C = C(t)$ and is determined by the volume of fluid present in the container, which is here assumed steady in time.

Linearized Governing Equations

Introducing the perturbation

$$h = H(x, y) + \eta(x, y, t), \tag{13}$$

normal modes are selected for ϕ and η such that

$$\phi = \phi'(x, y, z)\cos(\omega_i t), \tag{14}$$

$$\eta = \eta'(x, y)\sin(\omega_i t). \tag{15}$$

Substituting eqs. 13–15 into eq. 12, neglecting nonlinear terms, and noting $\omega_i = 0$ for neutral stability, yields the simplified Bernoulli equation

$$B(H + \eta) + \mathcal{L}(H + \eta) = C, \tag{16}$$

where the prime notation for η has been dropped for clarity. Assuming $\eta/H \ll 1$, the zeroeth order solution for the interface shape H may be determined from eq. 16 to be

$$BH + \mathcal{L}H = C, \tag{17}$$

where $\mathcal{L}H$ is the operation of eq. 9 on H. Eq. 17 is subject to

$$\pm\frac{\epsilon H_x}{\left(1+\epsilon^2 H_x^2+H_y^2\right)^{1/2}}=\cos\theta \qquad \text{along} \qquad x=\pm 1$$

and

$$\pm\frac{H_x}{\left(1+\epsilon^2 H_x^2+H_y^2\right)^{1/2}}=\cos\theta \qquad \text{along} \qquad y=\pm 1.$$

The first order solution for the perturbation η is given by

$$B\eta+\tilde{\mathcal{L}}\eta=0, \tag{18}$$

subject to

$$\epsilon\eta_x\left(1+H_y^2\right)-\epsilon\eta_y H_x H_y=0 \qquad \text{along} \qquad x=\pm 1$$

and

$$\eta_y\left(1+\epsilon^2 H_x^2\right)-\epsilon^2\eta_x H_x H_y=0 \qquad \text{along} \qquad y=\pm 1.$$

The operation $\tilde{\mathcal{L}}\eta$ is defined by

$$\begin{aligned}\tilde{\mathcal{L}}\eta=&\frac{1}{\left(1+\epsilon^2 H_x^2+H_y^2\right)^{3/2}}\Big[\epsilon^2\eta_{xx}\left(1+H_y^2\right)+\eta_{yy}\left(1+\epsilon^2 H_x^2\right)-2\epsilon^2\eta_{xy}H_x H_y\\&+2\epsilon^2\left(\eta_y H_{xx}H_y+\eta_x H_x H_{yy}-\eta_y H_x H_{xy}-\eta_x H_y H_{xy}\right)\Big]\\&-\frac{3\mathcal{L}H}{\left(1+\epsilon^2 H_x^2+H_y^2\right)}\left(\epsilon^2\eta_x H_x+\eta_y H_y\right),\end{aligned} \tag{19}$$

and is determined by expanding $\mathcal{L}(H+\eta)$ in powers of η retaining only terms of $O(\eta)$. In the limit $\epsilon^2 \ll 1$,

$$\tilde{\mathcal{L}}\eta=\frac{\eta_{yy}}{\left(1+H_y^2\right)^{3/2}}-\frac{3\eta_y H_y H_{yy}}{\left(1+H_y^2\right)^{5/2}},$$

subject to the leading order boundary condition $\eta_y=0$ on $y=\pm 1$, which recovers the governing system of Concus (1963) for the infinite slot. It is important to note that for this limiting case the first boundary condition to eq. 18 is $O(\epsilon)$ and is ignored. The infinite slot formulation is thus accurate to $O(\epsilon)$ for a finite slot provided $\theta \approx 90°$.

Numerical Solution Detail

In the numerical solution procedure eq. 17 is discretized based on a fourth-order central-differencing scheme. For the calculation of the static shape of the free surface $H(x,y;B)$, the Newton iteration method with successive under-relaxation is used to address the non-linearity of the governing equation. In determining the eigenvalue, $B=B_{cr}$, the same discretization as that used for solving the static interface shape is used and can be expressed in the following form

$$[\mathbf{A}+B\mathbf{I}]\,\eta=0. \tag{20}$$

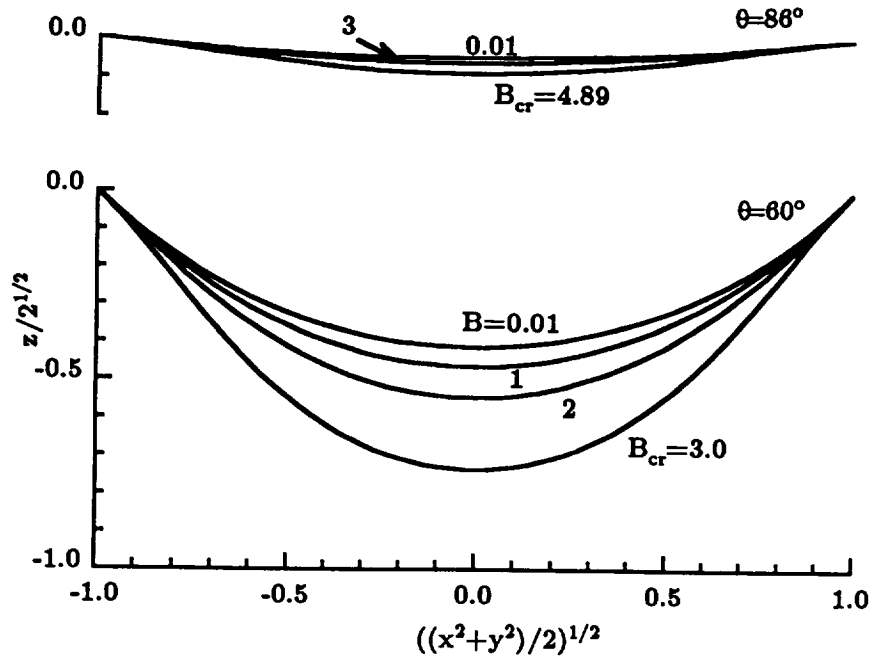

FIGURE 4. Surfaces profiles across container diagonal of a square container for a variety of contact angles and Bond numbers.

The determinant of the coefficient matrix in eq. 20 is zero at $B = B_{cr}$. Since the coefficient matrix [A] is dependent on the static shape and thus B, the overall solution procedure involves an iteration between eq. 20 via eq. 18 and the calculation of the static shape, eq. 17. A bisection method is used to determine B_{cr} in the iteration process. It should be noted that the determination of the critical Bond number has to be based on the solution from the full domain (*i.e.* all four solid boundaries included). This is due to the fact that an asymmetric disturbance leads to the fundamental subharmonic mode instability.

As θ decreases towards 45° (or increases towards 135°), the nonlinearity of the static eq. 17 increases dramatically, requiring a smaller relaxation factor for the Newton iterations. Hence, the run time per case increases as the contact angle deviates from 90°. For a 60×60 grid system, the typical run time per case on an SGI Indigo II with a single-processor is one hour for contact angles in the vicinity of 90°. However, the run time becomes significantly longer, reaching 24 hours, when the contact angle is close to 45°. Expectedly, solutions for B_{cr} are found to be symmetric about $\theta = 90°$.

RESULTS

In Fig. 4, surface profiles across the diagonal of a square cross-section container ($\epsilon = 1$) are compared for a variety of Bond numbers for contact angles 86° and 60°. The coordinates for the figure are normalized by the diagonal of the container and are presented to scale. The base-state interface shape $H(x, y)$ for the case $\epsilon = 1$, $\theta = 60°$ is presented 3-dimensionally in Fig. 5 for $B_{cr} = 3.0$. Slight inflections of the interface near the corners are observed which can also be discerned in Fig. 4, $\theta = 60°$, $B_{cr} = 3.0$. These appear to diminish with decreasing θ.

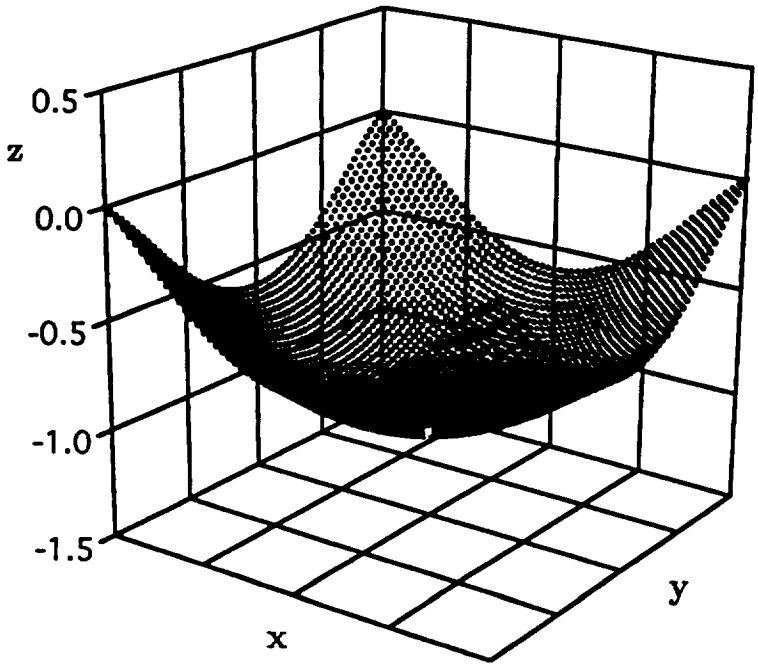

FIGURE 5. Surface shape $H(x, y; B_{cr})$ for $\theta = 60°$ in a square cross-sectioned container, $\epsilon = 1$.

The numerical results for B_{cr} are presented in Fig. 6 as a function of θ for the aspect ratio $\epsilon = 1$. The numerical results of Concus (1963) for the infinite slot and the right circular cylinder are also provided via eqs. 1 and 2. The region of stability denoted by the area below the curves is obviously altered for the rectangular section of this study when compared to the infinite slot. This is attributable to the restricted range of contact angles allowing for stable interfaces which cover the solution domain. Further "preliminary" calculations show that the rapid decrease of B_{cr} towards zero for $\theta \lesssim 48°$ reveals the sensitivity of the surface to the critical contact angle condition which is satisfied for $\theta \leq 45°$. This trend is indicated on Fig. 6 by the dashed line extrapolations from the numerical solutions obtained for $60° \lesssim \theta \lesssim 120°$. It is useful to note that for $\theta \gtrsim 48°$, B takes normally anticipated values, $O(1)$. The effect of contact angle hysteresis on such stability results is likely to delay the instability while equilibrium conditions are established at the contact line. If the disturbance has temporal periodicity, the effect of hysteresis could be to significantly increase the stability of the interface, particularly for contact angles near 45°. However, as found in recent space experiments by Concus *et al.* (1997), extended periods of thermal and mechanical disturbances in the presence of a steady background acceleration such that $B \gtrsim B_{cr}$ will ultimately bring about the predicted instability.

It is important to note that the rectangular geometry of this investigation is fundamentally different from the infinite rectangular slot as seen by the limiting case of $\epsilon \to 0$. One might expect the solution to agree in this limit, however, the presence of the corners dramatically alters the base state surface profile for $\theta \searrow 45°$, or $\theta \nearrow 135°$.

It is also of interest to note that an inflection point appears in the static interface

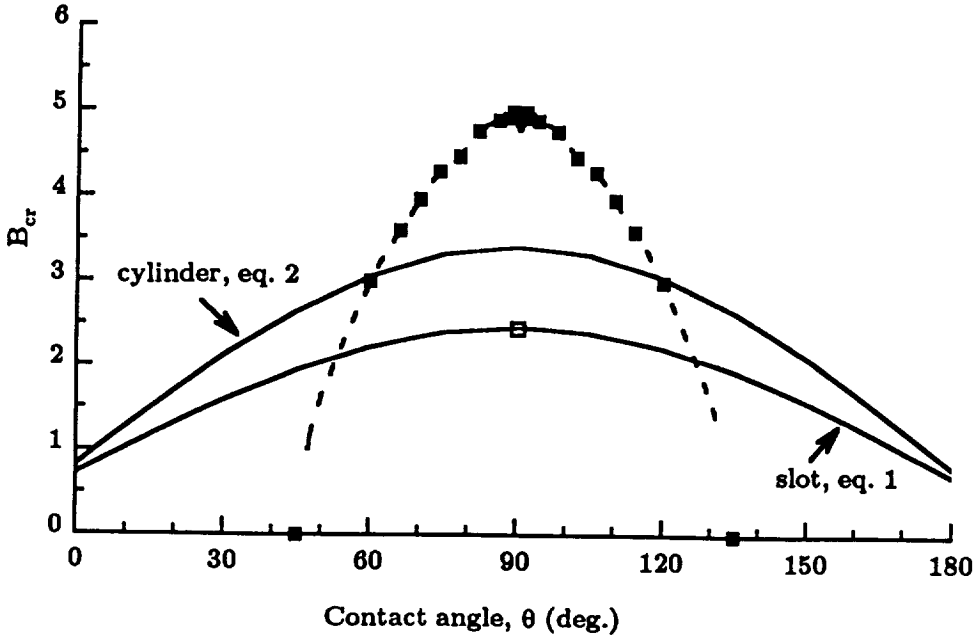

FIGURE 6. B_{cr} versus θ for $\epsilon = 1$; ■ numerical results, — eqs. 1 and 2 for the infinite rectangular slot and right circular cylinder, and $\triangledown$ and □ are eqs. 4 and 5 for the case $\epsilon = 1$, $\theta = 90°$, respectively. Dashed line is extrapolation of numerical results.

shape as a result of the additional space dimension in the solution of the problem in x and y. Such inflections are not found in the cases of the slot and the cylinder which are 1-dimensional problems where the onset of any inflection of the surface actually *signals* the onset of instability, Concus (1964).

The fact that B_{cr} determined numerically agrees with eq. 5 ($\triangledown$ on Fig. 6) in the limit $\theta \to 90°$ is expected and serves in part as a verification of the numerical results. The code was also "checked" using 90° contact angle conditions on opposing faces of the containers while varying θ on the other opposing faces. The results from these runs recovers the infinite slot results of Concus (1963) for all values of the contact angle. For the full numerical problem, however, for contact angles lower than $\approx 60°$, the numerical approach employed experiences convergence difficulties. What is observed is that for $\theta \lesssim 60°$ ($\theta \gtrsim 120°$) the L_2 norm ($\equiv ||H^{n+1} - H^n||$) of the base state eq. 17 decreases to a minimum and then proceeds to increase after excessive iterations without achieving machine zero. It is taken for granted that the steepening of the interface in the corner as the contact angle decreases, typified by the angle of the interface in the corner measured along the corner bisector $\theta_c = \cos^{-1}(\sqrt{2}\cos\theta)$, leads to increased grid resolution uncertainties, increased nonlinearities in the governing equations, and thus increased run time and roundoff errors. But these effects should not be appreciable for say $\theta \approx 55°$, where $\theta_c = 41°$. Since a slight variation in B_{cr} was also detected when $\theta \lesssim 60°$ for different values of the relaxation factor, it is our suspicion that the Newton iteration method with under-relaxation may not be the most robust technique for the system of equations solved herein. As a recourse, a time-marching scheme is presently being developed to further investigate the numerical issues.[1] Regardless, the qualitative nature of the computational results will remain unchanged as those presented in Fig. 6. With the numerical issues resolved, calculations for B_{cr} will be

[1]The dashed line extrapolations of Fig. 6 are actually numerical solution curves deemed "preliminary" in that these experience convergence difficulties.

completed for a range of aspect ratios, ϵ.

CONCLUSION

The governing equations and boundary conditions for the determination of the dynamic stability of capillary surfaces in rectangular containers are extended to 3-dimensions and presented for numerical solution. Calculations for a square cross-sectioned container are performed which serve as a model for containers possessing interior corners. Such container-types are commonly employed in fluids management systems in space. The results reveal that, though stability is comparable to the circular cylinder for large contact angles near 90°, the range of contact angles yielding positive values for the critical Bond number is significantly reduced due to a corner wetting phenomena governed by the Concus-Finn condition. B_{cr} is determined to be $O(1)$ for $48° \lesssim \theta \lesssim 132°$, but diminishes rapidly to zero as θ approaches 45° from above, or 135° from below. Computations addressing the effects of container aspect ratio ϵ are currently underway.

Acknowledgments

This work was supported by the Fluid Physics Branch of the Microgravity Science Division at NASA's Lewis Research Center. The authors wish to thank summer high school students C. Rogers, D. Swanson, and S. Harasim for assistance with the computations.

References

Concus, P. (1963) "Capillary Stability in an Inverted Rectangular Tank," *Advances in the Astronautical Sciences*, Western Periodicals Co., North Hollywood, CA, **14**:21–37.

Concus, P., Capillary stability in an inverted rectangular channel for free surfaces with curvature of changing sign, *AIAA J.*, **2**:12, 2229.

Concus, P. (1968) Static menisci in a vertical right circular cylinder, *J. Fluid Mech.*, **34**, 481–495.

Concus, P. and R. Finn (1969) On the Behavior of a Capillary Free Surface in a Wedge, *Proc. Nat. Acad. Sci. U.S.A.*, **63**, 292–299.

Concus, P. Finn, R., Weislogel, M. (1997) Measurement of critical contact angle in a microgravity experiment, *Experiments in Fluids* (submitted).

Coriell, S.R., S.C. Hardy, and M.R. Cordes (1977) Stability of liquid zones, *J. Colloid and Int. Sci.*, **60**:1, 126–136.

Duprez, M. (1854) Sur un cas particularier l equilibre des liquides, par F. Duprez, *Nouveaux Mem. de l'Acad. de Belgique.*

Labus, T.L. (1969) Natural frequency of liquids in annular cylinders under low gravity conditions, NASA TN D-5412.

Masica, W.J. and D.A. Petrash (1965) Hydrostatic stability of the liquid-vapor interface in a gravitational Field, NASA TN D-2267.

Masica, W.J., J.D. Derdul, and D.A. Petrash (1964) Hydrostatic stability of the liquid-vapor interface in a low-acceleration field, NASA TN D-2444.

Maxwell, J.C. (1890) Capillary action, in the Scientific Papers of James Clerk Maxwell, Cambridge University Press, London.

Reynolds, W.C. and H.M. Satterlee (1966) Liquid propellant behavior at low and zero g, in NASA SP-106, ed. H.N. Abramson, chpt. 11.

Seebold, J.G., M.P. Hollister, and H.M. Satterlee (1967) Capillary hydrostatics in annular tanks, *J. Spacecraft*, 4:1, 101–105.

Singh, B.S. (1996) Third Microgravity Fluid Physics Conference, NASA Conference Publication 3338, Workshop Proceedings, Cleveland, Ohio, July 13–15.

Wente, H.C. (1980) The stability of the axially symmetric pedant drop, *Pacific J. of Math.*, 88, 421–470.

Yiantsios, S.G., B.G. Higgins (1989) Hydrodynamic stability of an inverted liquid film, *Phys. Fluids A*, 1, 1484–1501.

REPORT DOCUMENTATION PAGE

Form Approved
OMB No. 0704-0188

1. AGENCY USE ONLY (*Leave blank*)	2. REPORT DATE	3. REPORT TYPE AND DATES COVERED
	January 1998	Technical Memorandum

4. TITLE AND SUBTITLE

Stability of Capillary Surfaces in Rectangular Containers: The Right Square Cylinder

5. FUNDING NUMBERS

WU-962-24-00-00

6. AUTHOR(S)

M.M. Weislogel and K.C. Hsieh

7. PERFORMING ORGANIZATION NAME(S) AND ADDRESS(ES)

National Aeronautics and Space Administration
Lewis Research Center
Cleveland, Ohio 44135-3191

8. PERFORMING ORGANIZATION REPORT NUMBER

E-11079

9. SPONSORING/MONITORING AGENCY NAME(S) AND ADDRESS(ES)

National Aeronautics and Space Administration
Washington, DC 20546-0001

10. SPONSORING/MONITORING AGENCY REPORT NUMBER

NASA TM—1998-206629

11. SUPPLEMENTARY NOTES

Responsible person, Mark M. Weislogel, organization code 6712, (216) 433-2877.

12a. DISTRIBUTION/AVAILABILITY STATEMENT

Unclassified - Unlimited
Subject Category: 64 Distribution: Nonstandard

This publication is available from the NASA Center for AeroSpace Information, (301) 621-0390.

12b. DISTRIBUTION CODE

13. ABSTRACT ***(Maximum 200 words)***

The linearized governing equations for an ideal fluid are presented for numerical analysis for the stability of free capillary surfaces in rectangular containers against unfavorable disturbances (accelerations, *i.e.* Rayleigh-Taylor instability). The equations are solved for the case of the right square cylinder. The results are expressed graphically in terms of a critical Bond number as a function of system contact angle. A critical wetting phenomena in the corners is shown to significantly alter the region of stability for such containers in contrast to simpler geometries such as the right circular cylinder or the infinite rectangular slot. Such computational results provide additional constraints for the design of fluids systems for space-based applications.

14. SUBJECT TERMS	15. NUMBER OF PAGES
Capillary surface; Stability; Microgravity; Contact angle, Surface tension	18
	16. PRICE CODE: A03

17. SECURITY CLASSIFICATION OF REPORT	18. SECURITY CLASSIFICATION OF THIS PAGE	19. SECURITY CLASSIFICATION OF ABSTRACT	20. LIMITATION OF ABSTRACT
Unclassified	Unclassified	Unclassified	